Mechanisms of Ageing and Development 232 (2026) 112194

Contents lists available at ScienceDirect

Mechanisms of Ageing and Development

journal homepage: www.elsevier.com/locate/mechagedev

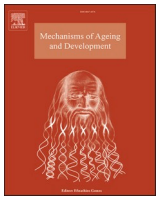

Pro-Xylane alleviates ultraviolet-induced skin senescence through SGK1-mediated p21 ubiquitination and subcellular translocation

Tingting Wang [a,b,*], Nan Huang [a,b], Xiaofang Zhang [c], Ting Yan [d]

[a] Department of Dermatovenereology, West China Hospital, Sichuan University, Chengdu, China
[b] Laboratory of Dermatology, Clinical Institute of Inflammation and Immunology (CIII), Frontiers Science Center for Disease-related Molecular Network, West China Hospital, Sichuan University, Chengdu, China
[c] Department of Dermatology, Mianyang 404 Hospital, Mianyang, Sichuan 621000, China
[d] Sichuan Botanee Biotechnology Co., Ltd, Chengdu, Sichuan 610000, China

ARTICLE INFO

Keywords:
Pro-Xylane
UVB
Skin senescence
SGK1
Ubiquitination

ABSTRACT

Background: Ultraviolet B (UVB) radiation causes skin damage, leading to aging and inflammatory responses. Pro-Xylane, a plant-derived compound, has been proposed for its potential protective effects against UVB-induced skin damage. However, its molecular mechanisms, particularly regarding cellular senescence, remain unclear.
Methods: HaCaT cells were exposed to UVB radiation and treated with Pro-Xylane. The effects on cell viability, apoptosis, reactive oxygen species (ROS) production, senescence markers, and collagen expression were assessed via CCK-8, TUNEL staining, DCFH-DA, and immunofluorescence assays. GEO datasets identified SGK1 as a key target. The p21 ubiquitination and subcellular localization were analyzed via immunoprecipitation and Western blot. In vivo experiments were conducted using UVB-irradiated rats to confirm the therapeutic effects of Pro-Xylane on skin regeneration.
Results: Pro-Xylane improved cell viability and inhibited ROS production in UVB-exposed HaCaT cells. Pro-Xylane decreased β-galactosidase expression and reversed UVB-induced upregulation of p21. SGK1 was identified as a key mediator in the protective effects. Pro-Xylane promoted mitochondrial function, and reduced oxidative stress. Mechanistically, Pro-Xylane promoted p21 ubiquitination (K141) and cytoplasmic retention, counteracting UVB-induced nuclear p21 accumulation.
Conclusion: Pro-Xylane effectively mitigated UVB-induced skin senescence and damage through SGK1-mediated p21 ubiquitination and subcellular translocation, making it a promising candidate for skin repair and anti-aging treatments.

1. Introduction

Skin, as the largest organ of the human body, serves as the primary defense against external environmental stressors (Jiao et al., 2024; Abdallah et al., 2017), with ultraviolet (UV) radiation (including UVA and UVB) being among the most harmful factors (Tang et al., 2024). UVB radiation, with a shorter wavelength and higher energy, penetrates the epidermis to induce direct DNA mutagenesis—particularly the formation of cyclobutane pyrimidine dimers (CPDs) and 6–4 photoproducts (6–4PPs)—which are key initiators of skin carcinogenesis (Pfeifer, 2020; Mallet et al., 2016). While oxidative damage and excessive reactive oxygen species (ROS)-mediated cellular macromolecule impairment are prominently associated with UVA radiation, UVB can also trigger ROS production via mitochondrial dysfunction or NADPH oxidase activation (Beak et al., 2004; Kim et al., 2023). UVB irradiation penetrates the epidermis, triggering a cascade of pathological responses, including DNA damage, cellular senescence, and apoptosis, which collectively contribute to skin aging, inflammation, and even carcinogenesis (Stasiewicz et al., 2023; Zhang et al., 2025; Panich et al., 2016). One of the hallmark features of UVB-induced skin aging is the breakdown of collagen and other extracellular matrix (ECM) proteins, which are crucial for maintaining skin structure and elasticity (Liu et al., 2025; Bar and Valiukevičienė, 2025). UVB exposure promotes the secretion of senescence-associated secretory phenotype (SASP) factors (e.g., TNF-α, MCP-1) by inducing cellular senescence, while also reducing collagen synthesis through upregulating matrix metalloproteinases (MMPs),

* Corresponding author at: Department of Dermatovenereology, West China Hospital, Sichuan University, Chengdu, China.
E-mail address: wangtingting817@126.com (T. Wang).

https://doi.org/10.1016/j.mad.2026.112194
Received 15 September 2025; Received in revised form 10 May 2026; Accepted 17 May 2026
Available online 20 May 2026

further impairing skin structure and function (Domaszewska-Szostek et al., 2021; Dorf and Maciejczyk, 2024).

To counteract the effects of UVB-induced skin damage, various preventive and therapeutic strategies have been explored. Among these, plant-derived compounds have garnered significant attention due to their antioxidant, anti-inflammatory, and skin-repairing properties (Zhao et al., 2025; Michalak, 2023). One such compound is Pro-Xylane, a natural sugar that has shown promise in enhancing skin hydration, improving barrier function, and promoting collagen synthesis (Zang et al., 2024). Pro-Xylane is known to regulate the synthesis of glycosaminoglycans (GAGs), which are essential components of the ECM, and its application has been linked to improved skin elasticity and reduced wrinkle formation (Dou et al., 2025; Bouloc et al., 2017). However, despite these promising findings, the precise mechanisms by which Pro-Xylane exerts its protective effects against UVB-induced skin damage remain unclear.

Serum- and glucocorticoid-inducible kinase 1 (SGK1), a serine/threonine kinase, regulates cellular responses to stress, ion homeostasis, and survival (E-Fatima et al., 2025; Yang et al., 2025). Dysregulated SGK1 expression has been linked to oxidative stress and inflammation (Liu et al., 2021; Jiang et al., 2019). Previous research found that the expression of SGK1 was upregulated in the aging-like skin in the UV-irradiated metabolic syndrome (MetS) mice (Nagase et al., 2013). And the topical application of mineralocorticoid receptor (MR) antagonist spironolactone inhibited SGK1 expression, oxidative stress, inflammation, and the aging-like changes in the skin (Nagase et al., 2013). Therefore, targeting SGK1 could offer a novel approach to protecting the skin from UVB-induced aging and damage. However, the potential of Pro-Xylane to modulate SGK1-mediated pathways and its effects on UVB-induced skin damage have not yet been fully explored. Additionally, p21, a cyclin-dependent kinase inhibitor, is a well-characterized senescence marker upregulated by UVB, which arrests cell cycle progression and promotes senescence (Ho and Dreesen, 2021; Yan et al., 2024a). Post-translational modifications, such as ubiquitination, and subcellular localization of p21 are critical for its function (Abbas and Dutta, 2009), but whether Pro-Xylane modulates these processes to alleviate UVB damage requires investigation.

In this study, we aimed to systematically evaluate the protective effects of Pro-Xylane against UVB-induced damage in HaCaT keratinocytes, primary human epidermal keratinocytes (HEKa), primary human dermal fibroblasts (HDF) and in a rat model of UVB-induced skin injury. Furthermore, we explored the underlying molecular mechanisms, focusing on the role of SGK1 and the regulation of p21 ubiquitination and subcellular localization. Our findings may reveal the therapeutic potential of Pro-Xylane in combating UVB-mediated skin aging and damage.

2. Materials and methods

2.1. Cell culture and treatment

HaCaT cells (a human keratinocyte cell line) were obtained from the Shanghai Cell Bank, Chinese Academy of Sciences (Shanghai, China) and cultured in Dulbecco's Modified Eagle's Medium (DMEM, 12491015, Gibco, MA, USA) supplemented with 10% fetal bovine serum (FBS, 10099158, Gibco, MA, USA) and 1% penicillin-streptomycin (15140122, Gibco, MA, USA) at 37°C in a humidified atmosphere containing 5% CO_2. Pro-Xylane was obtained from MedChemExpress (HY-108036B, Shanghai, China). For UVB exposure, the culture medium was removed, and cells were rinsed twice with phosphate-buffered saline (PBS). UVB irradiation was performed using a UVB lamp (SUV-1000, Sigma-Aldrich, Shanghai, China) at different intensities (0–50 mJ/cm^2). After irradiation, fresh culture medium containing Pro-Xylane (0, 100, 200, 400, 600, 800, 1000 μM) was added, and cells were incubated for 24 h before subsequent assays.

2.2. Primary human epidermal keratinocytes (HEKa) and primary human dermal fibroblasts (HDF) isolation

The isolation of primary HEKa and HDF was conducted using foreskin tissues obtained from healthy donors, as detailed in previous studies (Mieremet et al., 2017; El Ghalbzouri et al., 2009). The study protocol was approved by the Ethics Committee of West China Hospital, Sichuan University (Approval No.: 250721003), and written informed consent was obtained from the donors. Following the removal of adipose tissue, the dermis and epidermis were separated by incubating the skin overnight in a solution of dispase II at a concentration of 2.4 U/mL (40104ES60, Yeasen, China). The primary HEKa were subsequently isolated from the epidermis through treatment with 0.05% (w/v) trypsin and cultured following previously described methods (Mieremet et al., 2017; El Ghalbzouri et al., 2009). Primary HDF cells were extracted by incubating the dermis in a 3:1 (w/w) mixture of collagenase and dispase II for two hours at 37°C, with subsequent culturing as outlined in prior studies (Mieremet et al., 2017; El Ghalbzouri et al., 2009). All isolated primary cells underwent testing and were confirmed to be free of mycoplasma contamination.

2.3. Cell viability assay

Cell viability was evaluated using the CCK-8 assay. Briefly, HaCaT, HEKa and HDF cells were seeded in 96-well plates (1×10^4 cells/well). After treatment, 10 μL of CCK-8 solution (A311–01, Vazyme, Nanjing, China) was added to each well, and the plates were incubated at 37°C for 2 h. The absorbance at 450 nm was measured using a microplate reader (Bio-Rad, Hercules, CA, USA). Cell viability was calculated as a percentage relative to the control group.

2.4. 5-ethynyl-2′ -deoxyuridine (EDU) staining assay

For EDU staining of cell proliferation, following the EDU kit (E607204, Sangon, China) instructions, EDU working solution at a final concentration of 10 μM was added to cells 2 h before culture termination, then fixed, permeabilized, counterstained with DAPI (C1002, Beyotime, Shanghai, China) for 5 min, and proliferating cells were observed and counted under a fluorescence microscope (IX73, Olympus, Tokyo, Japan).

2.5. Cell apoptosis detection

Apoptotic cells were detected using the TdT mediated dUTP Nick End Labeling (TUNEL) assay. Cells were fixed with 4% paraformaldehyde (P1110, Solarbio, Beijing, China) for 30 min at room temperature, permeabilized with 0.1% Triton X-100 (P0096–100ml, Beyotime, Shanghai, China) for 5 min, and incubated with TUNEL reaction mixture (40306ES60, Yeasen, Shanghai, China) at 37°C for 1 h in the dark. Nuclei were counterstained with DAPI (C1002, Beyotime, Shanghai, China) for 5 min. Images were captured using a fluorescence microscope (IX73, Olympus, Tokyo, Japan), and the apoptotic rate was calculated as the percentage of TUNEL-positive cells relative to total DAPI-stained cells.

2.6. Measurement of senescence-associated secretory phenotype (SASP) factors and oxidative stress markers

The SASP factors levels were quantified using commercial enzyme-linked immunosorbent assay (ELISA) kits. Specifically, Monocyte chemoattractant protein-1(MCP-1, ab179886, Abcam, China), tumor necrosis factor-α (TNF-α, PT518, Beyotime, China), and transforming growth factor-β1 (TGF-β1, PT880, Beyotime, China) ELISA kits were utilized based on the manufacturer's protocols. HaCaT cells were treated with UVB (40 mJ/cm^2) followed by Pro-Xylane for 24 h. The cell culture supernatant was collected, and ELISA was performed to detect TNF-α,

MCP-1, and TGF-β1. For in vivo SASP factor detection, rat dorsal skin samples were homogenized to prepare lysates, and ELISA was performed to detect TNF-α, MCP-1, and TGF-β1. Absorbance was recorded using a microplate reader (Bio-Rad, Hercules, CA, USA). The levels of oxidative stress markers, including malondialdehyde (MDA, BC0025, Solarbio), reduced glutathione (GSH, BC1175, Solarbio), superoxide dismutase (SOD, BC0170, Solarbio) activity, were determined using commercial assay kits according to the manufacturer's instructions.

2.7. Reactive oxygen species (ROS) production detection

Intracellular ROS levels were measured using the 2′7′-Dichlorofluorescein diacetate probe (DCFH-DA, S0033S, Beyotime, Shanghai, China). After treatment, cells were incubated with 10 μM DCFH-DA in serum-free DMEM at 37°C for 30 min. Cells were then rinsed with PBS, and fluorescence intensity was detected using a fluorescence microscope. Relative ROS levels were quantified using ImageJ software.

2.8. β-galactosidase staining for senescence

Cellular senescence was assessed by β-galactosidase activity. Cells were fixed with 4% paraformaldehyde for 15 min, rinsed with PBS, and incubated with β-galactosidase staining solution (G1580, Solarbio, Beijing, China) at 37°C overnight in the dark. Stained cells were observed under a light microscope (BX 50, Olympus), and the senescence rate was calculated as the percentage of β-galactosidase-positive cells relative to total cells.

2.9. GEO dataset analysis

Three GEO datasets (GSE222414, GSE185320, GSE138800) were downloaded from the Gene Expression Omnibus (GEO) database (https://www.ncbi.nlm.nih.gov/geo/). Differential expressed genes (DEGs) between UVB-irradiated and control cells were identified using the limma package in R (adjusted $p < 0.05$, $|\log_2 FC = > 1.5)$. Batch effects between the datasets were removed using the "removeBatchEffect" method in the limma R package. Venn diagrams were constructed using the VennDiagram package to identify overlapping DEGs among the three datasets.

2.10. Plasmids construction and cell transfection

The SGK1 overexpression plasmid was constructed by inserting the full-length coding sequence of SGK1 into the pcDNA3.1 vector. Short hairpin RNAs (shRNAs) targeting SGK1 (sh-SGK1) and a non-targeting control shRNA (sh-NC) were designed and inserted into a pLKO.1 vector. The SGK1 shRNA sequences were represented in Table. S1. HaCaT cells were transfected with the plasmids using Lipofectamine 3000 (L3000015, Invitrogen, USA) at a 1:2 (w/w) DNA: lipid ratio according to the manufacturer's instructions. Transfection efficiency was confirmed through RT-PCR analysis using GAPDH as internal control (Fig.S1).

2.11. Reverse transcription-polymerase chain reaction (RT-PCR) analysis

Total RNA was extracted from cells using the RNA extraction kit (DP419, TIANGEN, Beijing, China), and cDNA was synthesized using a reverse transcription kit (RR037B, Takara, Dalian, China). RT-PCR was performed using SYBR Green Master Mix (RR067A, Takara) on an ABI 7900HT System (Applied Biosystems, USA). The primer sequences were as follows: SGK1: forward 5'-GCCTGCCGCCTTTTTATAGC-3', reverse 5'- AAGATGTCCTGTCAGCTGGC-3'; PCOLCE2: forward 5'- CGCTGCTGAACCAAACGAAA-3', reverse 5'- TTGTGATAACAGTGCCGGCT-3'; FRY: forward 5'-CAGAGCTCATCGCAAATGGC-3', reverse 5'- GGCAGTGCTGGTTTTCTTGG −3'; GAPDH: forward 5'-GATTTGGTCGTATTGGGCGC −3', reverse 5'-AGTGATGGCATGGACTGTGG-3'. Relative gene expression was calculated using the $2^{-}\Delta\Delta Ct$ method, with GAPDH as the internal reference.

2.12. Nuclear-cytoplasmic fractionation

Nuclear and cytoplasmic proteins were separated using a nuclear-cytoplasmic extraction kit (P0028, Beyotime) according to the manufacturer's protocol. Briefly, cells were harvested, resuspended in cytoplasmic extraction buffer, incubated on ice for 15 min, and centrifuged at 12,000 × g for 5 min to collect the cytoplasmic fraction (supernatant). The pellet was resuspended in nuclear extraction buffer, incubated on ice for 30 min, and centrifuged to collect the nuclear fraction (supernatant). Protein concentration was determined, and fractions were analyzed by Western blot.

2.13. Western blot analysis

Cell samples were lysed in RIPA buffer (P0013B, Beyotime, Shanghai, China) and the protein concentration was determined using the BCA assay kit (20200ES76, Yeasen, Shanghai, China). Equal amounts of protein (30 μg) were separated by 10% sodium dodecyl sulfate-polyacrylamide gel electrophoresis (SDS-PAGE) and transferred to polyvinylidene fluoride (PVDF) membranes (Merck, Darmstadt, Germany). Membranes were blocked with 5% non-fat milk in TBST for 1 h at room temperature, then incubated with primary antibodies including anti-SGK1 (ab32374, 1:500 dilution, Abcam, Shanghai, China), anti-p21 (ab109520, 1:1500 dilution, Abcam, Shanghai, China), anti-p16 (30519–1-AP, 1:2000 dilution, Proteintech, Wuhan, China), anti-β-actin (AF7018, 1:3000 dilution, Affinity, Shanghai, China), anti-Lamin B1 (AF5161, 1:2000 dilution, Affinity, Shanghai, China), anti-Ubiquitin (ab303664, 1:1000 dilution, Abcam, Shanghai, China) and anti-GAPDH (ab9485, 1:2500 dilution, Abcam, Shanghai, China) overnight at 4°C, followed by HRP-conjugated secondary antibodies (1:5000 dilution) for 1 h at room temperature. Protein bands were detected through enhanced chemiluminescence (Pierce, MA, USA) and imaged using a FluorChem system (Bio-Rad Laboratories, CA, USA).

2.14. Mito-Tracker staining for mitochondria and mitochondrial membrane potential (MMP) detection

Mitochondria were labeled using Mito-Tracker Green (C1048, Beyotime). Cells were incubated with 100 nM Mito-Tracker Green at 37°C for 30 min, rinsed with PBS, and observed under a fluorescence microscope. MMP was detected using the JC-1 probe (C2006, Beyotime). The cells were incubated with 5 μM JC-1 at 37°C for 20 min, rinsed with PBS, and fluorescence (red for aggregated JC-1 in healthy mitochondria, green for monomeric JC-1 in depolarized mitochondria) was detected using a fluorescence microscope. The MMP ratio (red/green fluorescence intensity) was calculated using ImageJ.

2.15. Immunoprecipitation assay

Immunoprecipitation assay was performed using the Immunoprecipitation Kit (C600689, Sangon, Shanghai, China). Cells were lysed in RIP lysis buffer, and the lysate was incubated with an anti-p21 antibody (ab109520, 1:100 dilution, Abcam, Shanghai, China) or normal IgG (ab172730, 1:200 dilution, Abcam, Shanghai, China) overnight at 4°C, then with Protein A/G agarose beads (P2055–10ml, Beyotime) for 4 h. Beads were washed 5 times with IP buffer, and bound proteins were eluted by boiling in SDS loading buffer. Eluted proteins were analyzed by Western blot using anti-ubiquitin antibody.

2.16. Site-directed mutagenesis of p21

Potential ubiquitination sites of p21 were predicted using the CPLM database (https://cplm.biocuckoo.cn/index.php). Site-directed mutagenesis of p21 (K16R, K75R, K141R, K154R, K161R, K163R) was

performed using the QuikChange Lightning Site-Directed Mutagenesis Kit (210519, Agilent Technologies, CA, USA) according to the manufacturer's instructions. The site-directed mutagenesis was performed to substitute lysine (K) with arginine (R) (conservative mutation, preserving protein structure but abolishing ubiquitination). Mutant plasmids were transfected into HaCaT cells using Lipofectamine 3000. At 48 h post-transfection, immunoprecipitation assay was performed as described to detect p21 ubiquitination.

2.17. Skin photoaging rat model

The male Sprague-Dawley (SD) rats (8-week-old, 200 ± 20 g) purchased from Cavens Experimental Animal Center (Changzhou, China). The rats were housed under standard conditions with controlled temperature and lighting, randomly assigned to experimental groups. Male SD rats were selected to avoid the potential influence of the estrogen cycle in female animals on skin condition and inflammatory response, ensuring experimental consistency. All experimental procedures were approved by the Ethics Committee of West China Hospital, Sichuan University (Approval No.: 250721003). The skin areas, each measuring 2 cm × 2 cm, were selected from the dorsal skin of each rat, and the hair at the sampling sites was shaved. The rats were divided into five groups (n = 6 per group): control group; UVB group, irradiated with UVB (150 mJ/cm^2, 3 times per week for 6 weeks); UVB+PBS group, which received PBS alone after UVB exposure; UVB+ Low-dose (1.0 mg/mL) Pro-Xylane group, which received topical low-dose Pro-Xylane after UVB exposure; and UVB+ High-dose (2.0 mg/mL) Pro-Xylane group, treated with high-dose Pro-Xylane post-UVB. Pro-Xylane solutions at different concentrations were applied topically after UVB exposure (0.2 mL per rat). Pro-Xylane was dissolved in phosphate-buffered saline (PBS) to form an aqueous solution for topical application. UVB exposure was conducted using specialized equipment with anti-UV stickers to shield nonexposed areas. Skin samples were harvested 48 h after the last UVB irradiation. At the experiment's conclusion, the animals were euthanized, and dorsal skin samples were collected for following histological staining.

2.18. Histological analysis and immunofluorescence assay

Skin samples were fixed in 4% paraformaldehyde, embedded in paraffin, and sectioned (4 μm). Hematoxylin and eosin (HE) staining (G1120, Solarbbio, Beijing, China) was performed to evaluate histological changes under a light microscope. For immunofluorescence, paraffin sections or cells were deparaffinized/rehydrated, antigen-retrieved, and blocked with 5% BSA for 1 h. Sections were incubated with primary antibodies including anti-Ki67 (ab15580, 1:500 dilution, Abcam, Shanghai, China), anti-p21 (ab109520, 1:200 dilution, Abcam, Shanghai, China), anti-p16 (30519–1-AP, 1:500 dilution, Proteintech, Wuhan, China), anti-Collagen I (ab138492, 1:1500 dilution, Abcam, Shanghai, China) and anti-Collagen III (ab184993, 1:100 dilution, Abcam, Shanghai, China) at 4°C overnight, followed by the secondary antibodies (1:500 dilution) for 1 h at room temperature. Nuclei were counterstained with DAPI. Images were captured using a fluorescence microscope (IX73, Olympus, Tokyo, Japan), and fluorescence intensity was quantified using ImageJ.

2.19. Statistical analysis

All experiments were performed in triplicate, and data are presented as mean ± standard deviation (SD). Statistical analysis was performed using GraphPad Prism 8.0 software. Differences between groups were analyzed by one-way analysis of variance (ANOVA) followed by Tukey's post-hoc test. A P-value less than 0.05 was considered statistically significant.

3. Results

3.1. Pro-Xylane ameliorates UVB-induced cell death in HaCaT cells in vitro

The molecular structure of Pro-Xylane was presented in Fig. 1A. To determine the optimal UVB intensity, HaCaT cells were exposed to varying doses of UVB, and cell viability was assessed using the CCK-8 assay. As shown in Fig. 1B, UVB exposure led to a gradual reduction in HaCaT cell viability with increasing irradiation intensity. Based on the results, 40 mJ/cm^2 was selected for subsequent experiments. HaCaT cells were treated with different concentrations of Pro-Xylane, and cell viability was measured via CCK-8. The results (Fig. 1C) demonstrated that Pro-Xylane at concentrations ranging from 100 to 1000 μM had no significant effect on the viability of normal HaCaT cells, confirming its safety. Subsequently, HaCaT cells were irradiated with UVB followed by treatment with various concentrations of Pro-Xylane. CCK-8 results revealed that UVB exposure significantly decreased cell viability, while Pro-Xylane treatment markedly promoted cell viability recovery (Fig. 1D). TUNEL staining (Fig. 1E-F) further showed that UVB irradiation significantly increased the apoptosis of HaCaT cells, whereas Pro-Xylane (800 and 1000 μM) notably alleviated UVB-induced damage and inhibited cell apoptosis. EDU staining unveiled that Pro-Xylane (800 and 1000 μM) significantly promoted UVB-suppressed cell proliferation of HaCaT (Fig. 1G-H) cells. Furthermore, intracellular reactive oxygen species (ROS) levels were detected using the DCFH-DA probes. Compared with the control group, UVB exposure significantly enhanced ROS production, and this effect was reversed by Pro-Xylane treatment, which remarkably suppressed ROS generation in HaCaT (Fig. 1I-J). To assess cellular senescence, β-galactosidase expression was detected using a β-galactosidase staining kit (Fig. 1K-L). UVB irradiation notably upregulated β-galactosidase expression in HaCaT cells, an effect that was significantly inhibited by Pro-Xylane. Consistently, double immunofluorescence staining for the senescence marker p21 and p16 showed that UVB-induced co-expressed p21/p16 was markedly reversed by Pro-Xylane (white arrow indicating the co-expression of p21/p16) (Fig. 1M-N).

3.2. Pro-Xylane suppresses UVB-induced cell death in primary HEKa and HDF cells in vitro

Next, we investigated the effects of Pro-Xylane on primary HEKa and HDF cells. Initial CCK-8 assays confirmed that Pro-Xylane (100–1000 μM) exhibited no cytotoxicity in normal primary cells (Fig. 2A-B). Following a dose-response optimization showing a gradual viability decline post-UVB exposure (Fig. 2C-D), an optimal intensity of 40 mJ/cm^2 was selected for subsequent experiments. Notably, Pro-Xylane treatment effectively reversed the UVB-induced reduction in cell viability (Fig. 2E-F), as evidenced by EdU staining at 800 and 1000 μM (Fig. 2G-J). Furthermore, DCFH-DA probe analysis revealed that Pro-Xylane remarkably abrogated the UVB-triggered accumulation of intracellular ROS (Fig. 2K-M). We next assessed cellular senescence phenotypes. The results demonstrated that Pro-Xylane significantly attenuated the UVB-induced upregulation of β-galactosidase activity in both cell types (Fig. 2N-P). Consistently, double immunofluorescence staining confirmed that the UVB-induced co-expression of senescence markers p21 and p16 was markedly reversed by Pro-Xylane treatment (white arrow indicating the co-expression of p21/p16) (Fig. 2Q-S).

3.3. SGK1 is identified as a key mediator of Pro-Xylane's protective effects

To explore potential molecular targets, differential gene expression in UVB-irradiated skin was analyzed using three GEO datasets (GSE222414, GSE185320, GSE138800) (Fig. 3A). Venn intersection analysis identified three overlapping genes: PCOLCE2, FRY, and SGK1.

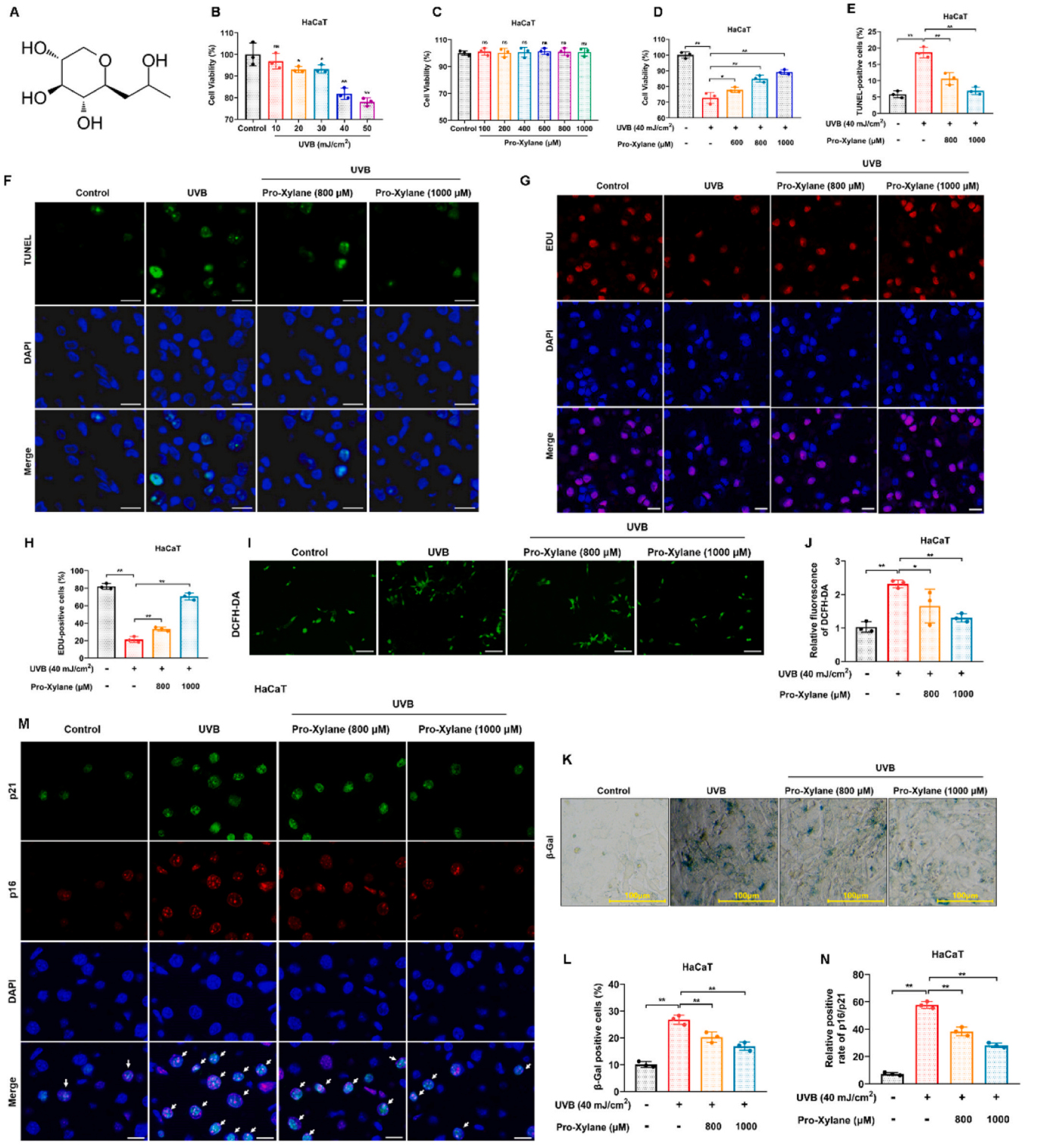

Fig. 1. Pro-Xylane ameliorates UVB-induced cell death in HaCaT cells in vitro. (A) Chemical structure of Pro-Xylane. (B) HaCaT cells were exposed to gradient doses of UVB, and cell viability was measured by CCK-8 assay (n = 3). (C) CCK-8 assay showing the effect of different concentrations of Pro-Xylane (100–1000 μM) on the viability of normal HaCaT cells (n = 3). (D) CCK-8 analysis of cell viability in UVB-irradiated HaCaT cells following treatment with Pro-Xylane (n = 3). (E-F) TUNEL staining and quantitative analysis in HaCaT cells (n = 3). Scale bar= 20 μm. (G-H) EDU staining was used to examine cell proliferation (n = 3). Scale bar= 20 μm. (I-J) Intracellular ROS levels detected by DCFH-DA probes (n = 3). Scale bar= 100 μm. (K-L) β-galactosidase staining and quantification (n = 3). Scale bar= 100 μm. (M-N) Double immunofluorescence staining for co-expression of p21 and p16 (n = 3). White arrow indicating the co-expression of p21/p16. Scale bar= 20 μm. Data were presented as mean ± SD; *P < 0.05, **P < 0.01. ns=non-significant.

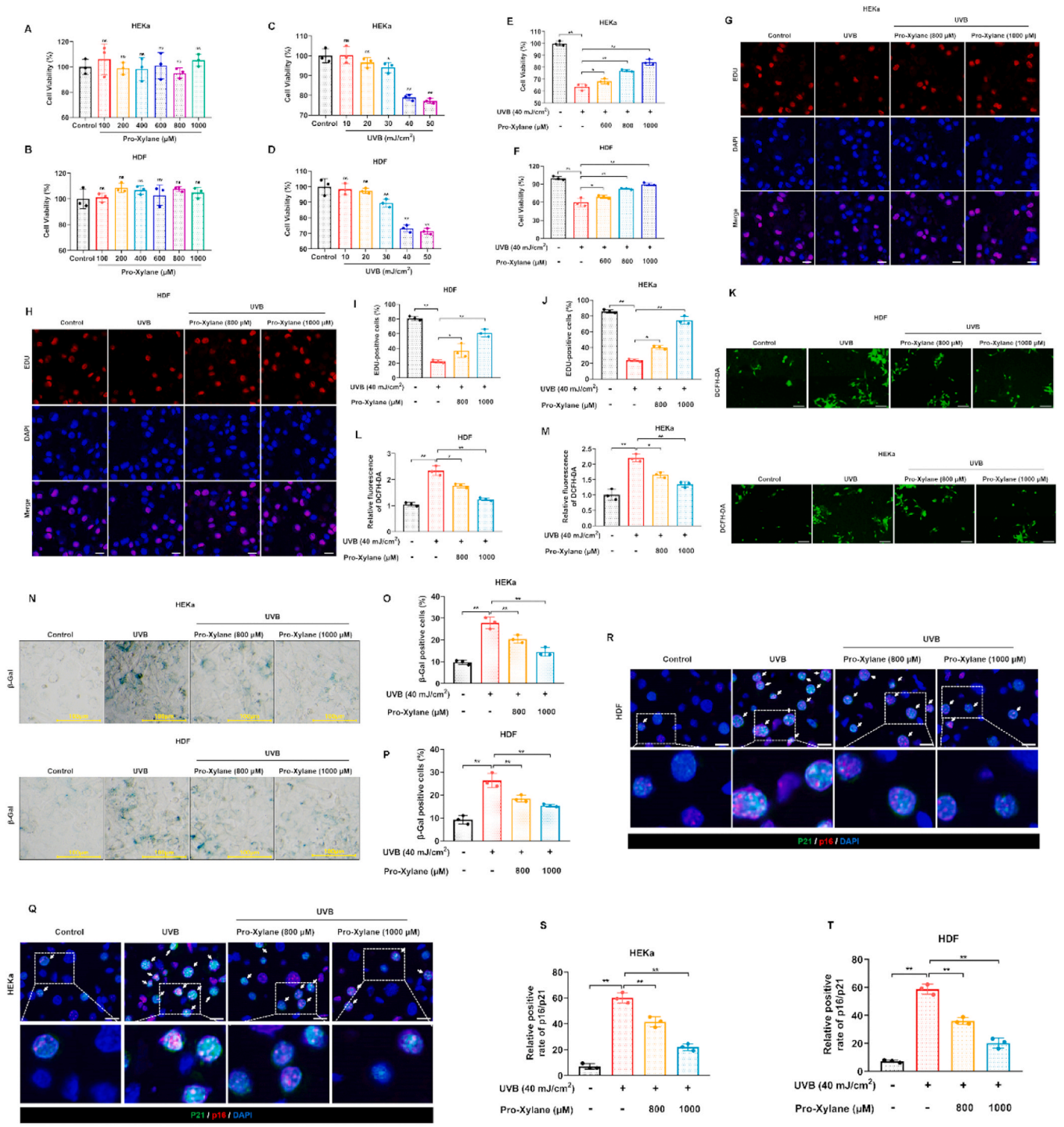

Fig. 2. Pro-Xylane suppresses UVB-induced cell death in primary HEKa and HDF cells in vitro. (A-B) CCK-8 assay showing the effect of different concentrations of Pro-Xylane (100–1000 μM) on the viability of HEKa and HDF cells (n = 3). (C-D) HEKa and HDF cells were exposed to gradient doses of UVB, and cell viability was measured by CCK-8 assay (n = 3). (E-F) CCK-8 analysis of cell viability in UVB-irradiated HEKa and HDF cells following treatment with Pro-Xylane (n = 3). (G-J) EDU staining was used to examine cell proliferation (n = 3). Scale bar= 20 μm. (K-M) Intracellular ROS levels detected by DCFH-DA probes (n = 3). Scale bar= 100 μm. (N-P) β-galactosidase staining and quantification (n = 3). Scale bar= 100 μm. (Q-S) Double immunofluorescence staining for co-expression of p21 and p16 (n = 3). White arrow indicating the co-expression of p21/p16. Scale bar= 20 μm. Data were presented as mean ± SD; *P < 0.05, **P < 0.01. ns=non-significant.

RT-PCR validation (Fig. 3B-D) revealed that UVB irradiation significantly upregulated SGK1 expression in HaCaT cells compared with the control group, while Pro-Xylane treatment significantly inhibited this upregulation, suggesting that the suppression of SGK1 is essential for Pro-Xylane to exert its protective effects against UVB-induced skin damage. Western blot analysis confirmed these findings, showing that UVB-induced upregulation of SGK1 protein levels was significantly reversed by Pro-Xylane (Fig. 3E-F). The SGK1 overexpression vector (SGK1-OE) and sh-SGK1 was constructed and transfected into HaCaT cells. CCK-8 and TUNEL staining assays demonstrated that Pro-Xylane significantly reversed UVB-induced reductions in cell viability (Fig. 3G) and increases in apoptosis (Fig. 3H-I). However, SGK1 overexpression significantly attenuated these protective effects of Pro-Xylane, leading to decreased cell viability and increased apoptosis.

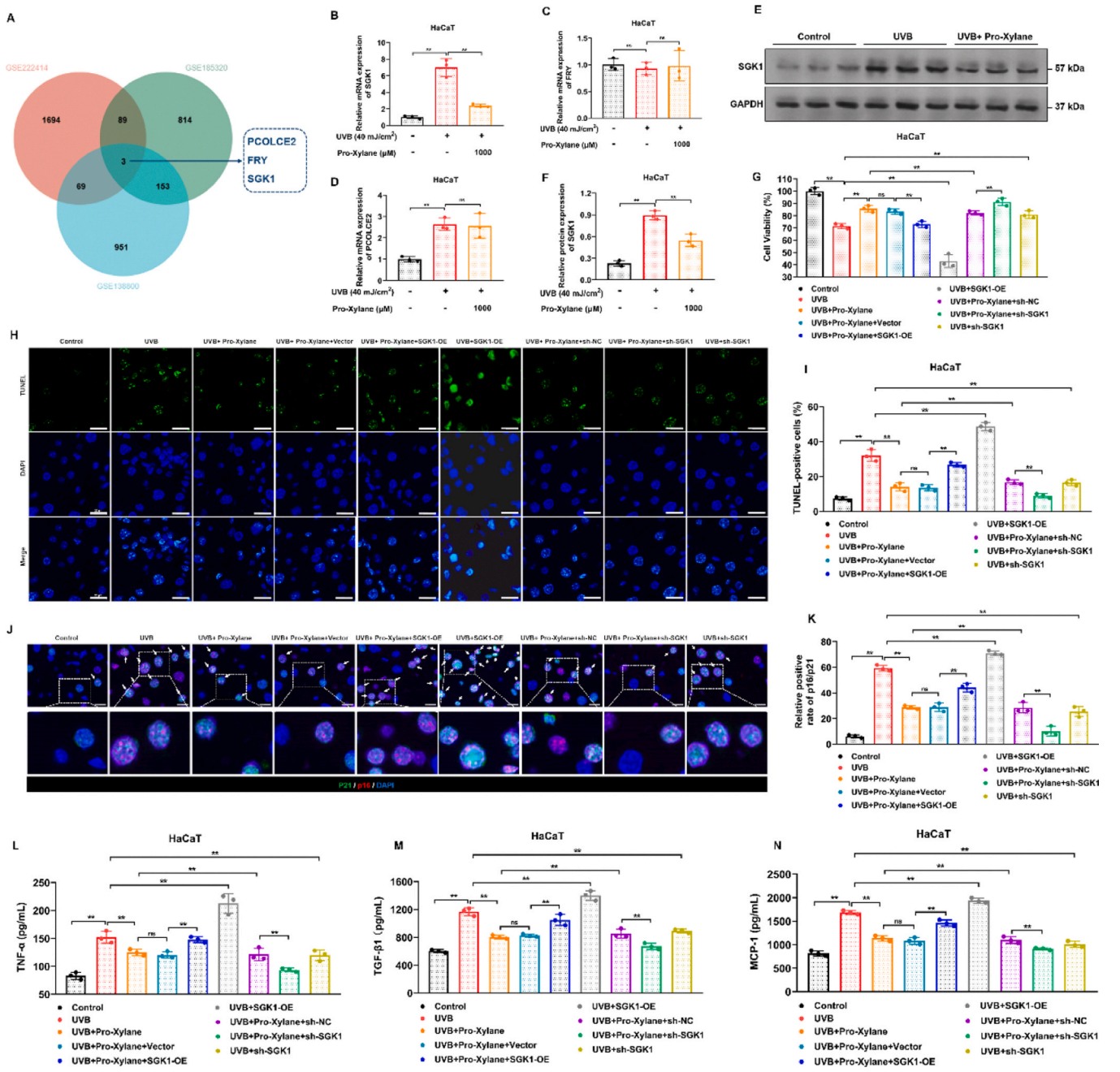

Fig. 3. SGK1 is identified as a key mediator of Pro-Xylane's protective effects. (A) Venn diagram showing overlapping differentially expressed genes identified by GEO datasets (GSE222414, GSE185320, GSE138800). (B-D) RT-PCR validation of PCOLCE2 (B), FRY (C), and SGK1 (D) expression in UVB-irradiated HaCaT cells with or without Pro-Xylane treatment (n = 3). (E-F) Western blot analysis detection the level of SGK1 expression (n = 3). (G) CCK-8 assay determination of cell viability (n = 3). (H-I) TUNEL staining and quantification of cell apoptosis (n = 3). Scale bar= 20 μm. (J-K) Double immunofluorescence staining and quantification for p21/p16 expression (n = 3). Scale bar= 20 μm. (L-N) Analysis of SASP factors (TNF-α, MCP-1, TGF-β1) using assay kits (n = 3). Data were presented as mean ± SD; **P < 0.01. ns=non-significant.

Knockdown of SGK1 enhanced the effects of Pro-Xylane, further increasing cell viability and inhibiting cell apoptosis. The double immunofluorescence staining for p21/ p16 (Fig. 3J-K) revealed that Pro-Xylane reversed UVB-induced co-expression of p21 and p16, an effect that was abrogated by SGK1 overexpression. While knockdown of SGK1 enhanced the effects of Pro-Xylane, further inhibiting the expression of p21 and p16. Additionally, assessment of senescence-associated secretory phenotype (SASP) showed that Pro-Xylane significantly reduced UVB-induced upregulation of TNF-α, MCP-1, and TGF-β1 (Fig. 3L-N), while SGK1 overexpression reversed this effect, promoting the upregulation of these SASP factors. Knockdown of SGK1 enhanced the effects of Pro-Xylane, further decreasing the levels of TNF-α, MCP-1, and TGF-β1.

3.4. Pro-Xylane regulates oxidative stress, mitochondrial function via SGK1

Intracellular ROS levels, assessed using the DCFH-DA probe, showed that Pro-Xylane inhibited UVB-induced ROS accumulation, while SGK1 overexpression reversed this effect, leading to increased ROS production

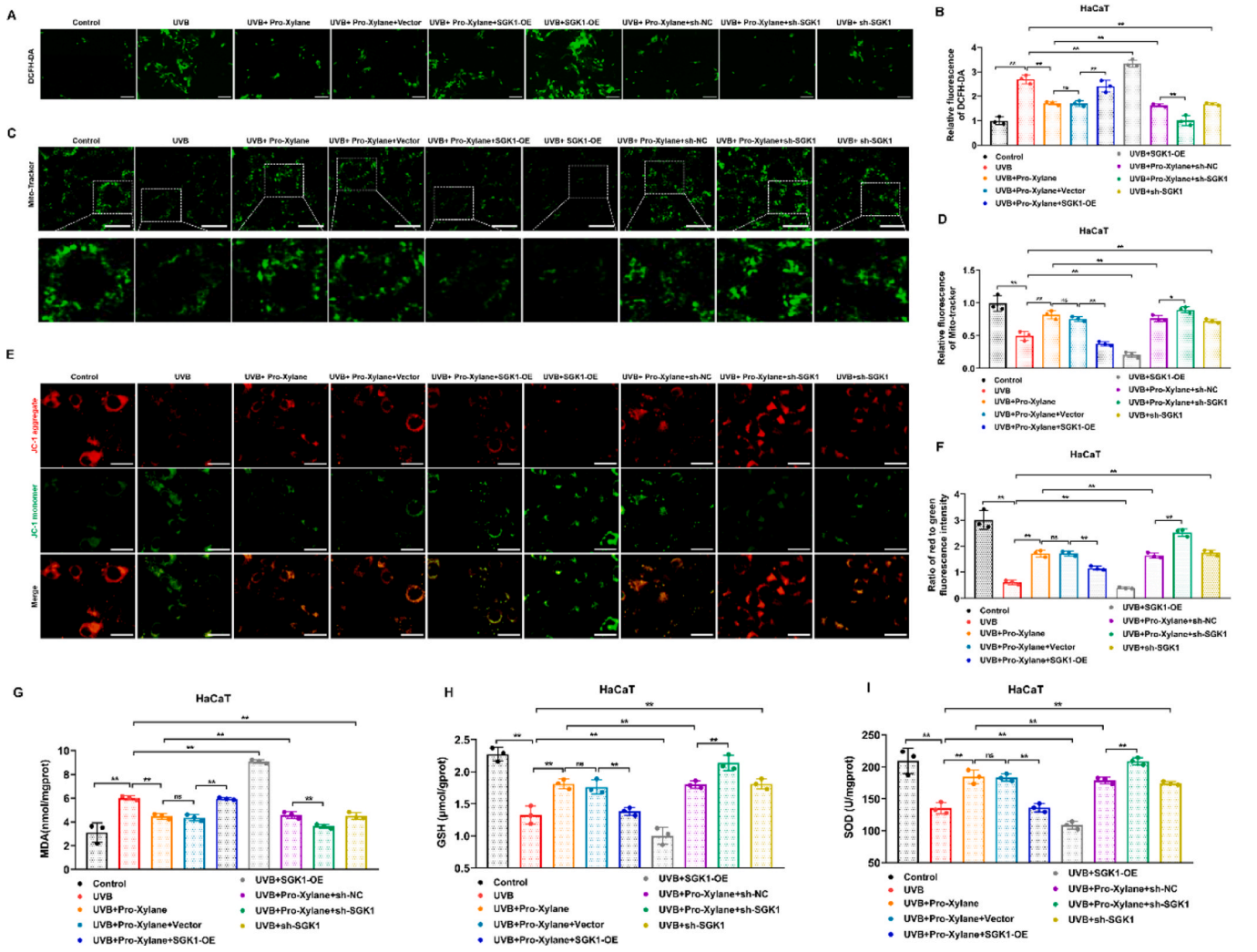

Fig. 4. Pro-Xylane regulates oxidative stress, mitochondrial function via SGK1. (A-B) DCFH-DA probe detection and quantification of intracellular ROS levels (n = 3). Scale bar= 100 μm. (C-D) Mito-Tracker staining labeled mitochondria (n = 3). Scale bar= 20 μm. (E-F) JC-1 probe analysis detection of mitochondrial membrane potential (MMP) (n = 3). Scale bar= 20 μm. (G-I) Assays of oxidative stress markers of MDA levels (G) and GSH (H) and SOD (I) activities (n = 3). Data were presented as mean ± SD; **P < 0.01. ns=non-significant.

(Fig. 4A-B). Knockdown of SGK1 enhanced the effects of Pro-Xylane, further inhibiting the ROS accumulation. Mitochondria and mitochondrial membrane potential (MMP) were evaluated using Mito-Tracker (Fig. 4C-D) and JC-1 probes (Fig. 4E-F), respectively. UVB irradiation inhibited Mito-Tracker fluorescence and reduced MMP, which were reversed by Pro-Xylane. While SGK1 overexpression attenuated these protective effects, resulting in decreased Mito-Tracker fluorescence and MMP. The transfection of sh-SGK1 further promoted the Pro-Xylane-induced Mito-Tracker fluorescence and MMP. Analysis of oxidative stress markers showed that Pro-Xylane inhibited malondialdehyde (MDA) levels (Fig. 4G) and activated glutathione (GSH) (Fig. 4H) and superoxide dismutase (SOD) (Fig. 4I) levels, while SGK1 overexpression significantly reversed these effects. Down-regulation of SGK1 further enhanced the impact of Pro-Xylane, inhibiting the level of MDA while promoting GSH and SOD activity.

3.5. Pro-Xylane modulates p21 ubiquitination and subcellular localization via SGK1

To explore the mechanism underlying Pro-Xylane's regulation of p21, nuclear and cytoplasmic proteins were isolated, and p21 subcellular distribution was detected by Western blot. As shown in Fig. 5A-F, UVB irradiation significantly promoted nuclear p21 expression and reduced cytoplasmic p21 levels compared with the control group. Pro-Xylane treatment reversed these effects, increasing cytoplasmic p21 and decreasing nuclear p21. While SGK1 overexpression attenuated this regulation, leading to increased nuclear p21 and decreased cytoplasmic p21. Knockdown of SGK1 further enhanced the impact of Pro-Xylane, promoting the cytoplasmic p21 and decreasing nuclear p21. Immunoprecipitation with the p21 antibody followed by ubiquitin immunoblotting revealed that UVB irradiation significantly inhibited p21 ubiquitination compared with the control group, while Pro-Xylane treatment reversed this inhibition, promoting p21 ubiquitination. SGK1 overexpression attenuated this effect, reducing p21 ubiquitination (Fig. 5G-H). Down-regulation of SGK1 further promoted p21 ubiquitination. Potential ubiquitination sites of p21 were predicted using the CPLM database (https://cplm.biocuckoo.cn/index.php), identifying six candidate sites: K16, K75, K141, K154, K161, and K163 (Fig. 5I). Site-directed mutagenesis was performed to construct p21 mutants (HA-p21-K16R, HA-p21-K75R, HA-p21-K141R, HA-p21-K154R, HA-p21-K161R, HA-p21-K163R). After transfection into HaCaT cells, immunoprecipitation with an HA antibody followed by ubiquitin immunoblotting showed that the K141R mutation significantly reduced ubiquitination levels (Fig. 5J), indicating that K141 is a critical ubiquitination site of p21.

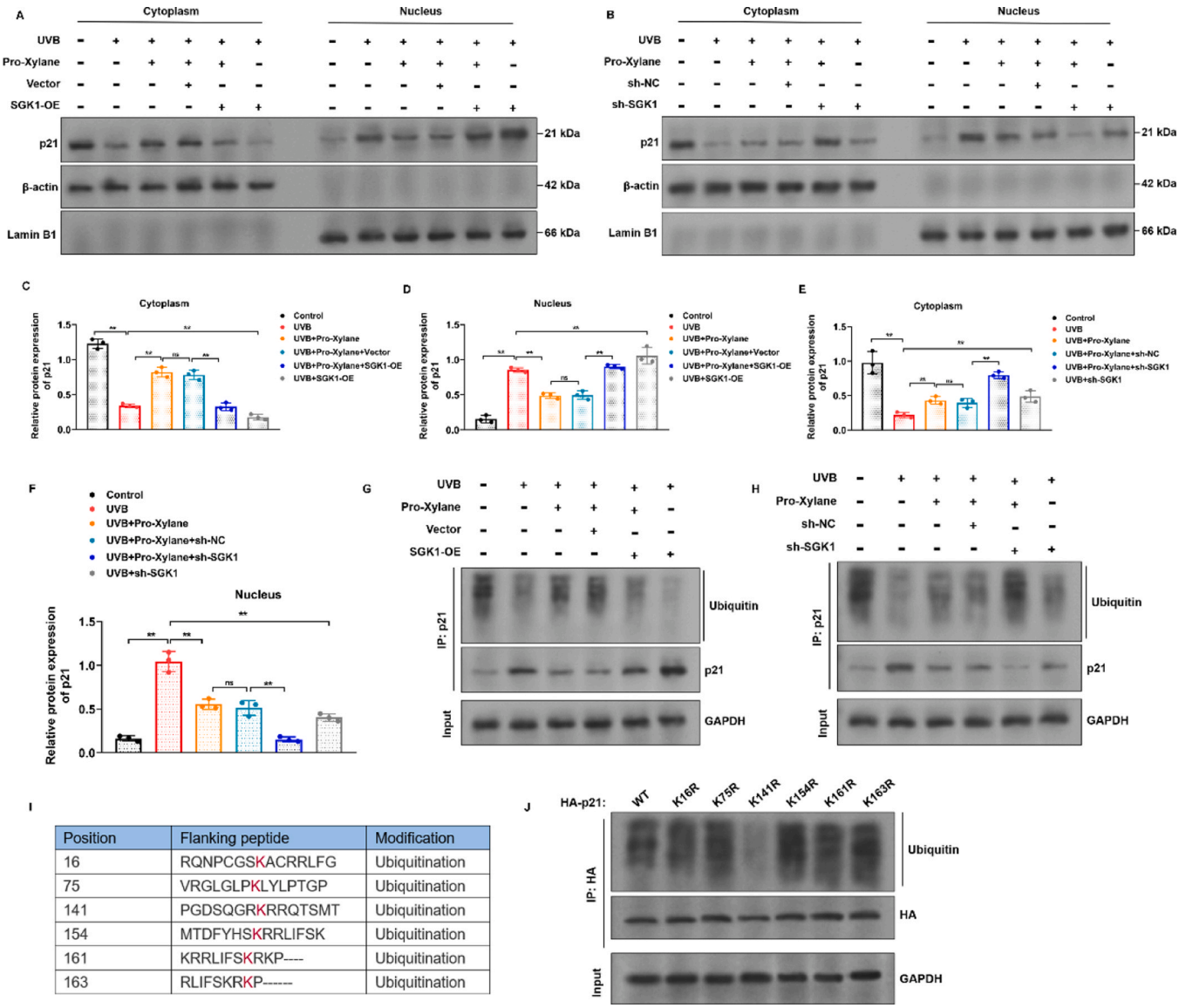

I

Position	Flanking peptide	Modification
16	RQNPCGSKACRRLFG	Ubiquitination
75	VRGLGLPKLYLPTGP	Ubiquitination
141	PGDSQGRKRRQTSMT	Ubiquitination
154	MTDFYHSKRRLIFSK	Ubiquitination
161	KRRLIFSKRKP----	Ubiquitination
163	RLIFSKRKP------	Ubiquitination

Fig. 5. Pro-Xylane modulates p21 ubiquitination and subcellular localization via SGK1. (A-F) Western blot analysis and quantification of nuclear and cytoplasmic p21 expression (n = 3). (G-H) Immunoprecipitation with the p21 antibody followed by ubiquitin immunoblotting (n = 3). (I) Prediction of p21 ubiquitination sites via the CPLM database, identifying K16, K75, K141, K154, K161, and K163 as candidates. (J) Ubiquitination assay of p21 mutants (K16R, K75R, K141R, K154R, K161R, K163R) (n = 3). Data were presented as mean ± SD; **P < 0.01. ns=non-significant.

3.6. Pro-Xylane ameliorates UVB-induced skin senescence and damage in vivo

In vivo experiments were conducted to confirm Pro-Xylane's prevention functions on UVB-induced skin senescence and damage. Preliminary experiments were performed to determine the optimal UVB intensity for inducing skin photoaging. The rats were irradiated with UVB at 80, 100, and 150 mJ/cm^2 (3 times per week for 6 weeks). HE staining (Fig. 6A-B) revealed that compared to the control group, UVB irradiation intensity (80, 100, 150 mJ/cm^2) significantly increased the thickness of epidermis, with the 150 mJ/cm^2 showing the most significant effect. Therefore, we chose 150 mJ/cm^2 for subsequent experiments. Fig. 6C illustrated the animal experimental process: rats were exposed to UVB on the dorsal skin, followed by treatment with Pro-Xylane (1.0 mg/mL and 2.0 mg/mL). HE staining of rat skin samples (Fig. 6D-E) showed that the UVB-irradiated group exhibited significant damage compared with the control group, with thickened epidermis (white arrow indicating the thickening of the epidermis). In contrast, high- and low-dose Pro-Xylane groups significantly inhibited epidermis thickening compared with the UVB group. Assessment of SASP factors revealed that Pro-Xylane significantly reduced UVB-induced upregulation of TNF-α, MCP-1, and TGF-β1 (Fig. 6F-H). Moreover, Western blot assay was applied to examine the expression of p21 and p16. As shown in Fig. 6I-J, Pro-Xylane significantly suppressed the expression of p21 and p16 which were induced by UVB. Moreover, double immunofluorescence staining confirmed that UVB-induced p16/p21 expression was mainly localized in epidermal keratinocytes. And the UVB-induced co-expression of senescence markers p21 and p16 was markedly reversed by Pro-Xylane treatment. Immunofluorescence staining for the Collagens I and III showed that UVB irradiation significantly downregulated Collagen I, and Collagen III levels compared with the control group. Pro-Xylane treatment reversed these effects, promoting Collagen I, and Collagen III expression (Fig. 6M-P).

4. Discussion

UVB radiation-induced skin damage remains a critical concern in dermatology, characterized by oxidative stress, cellular senescence, and

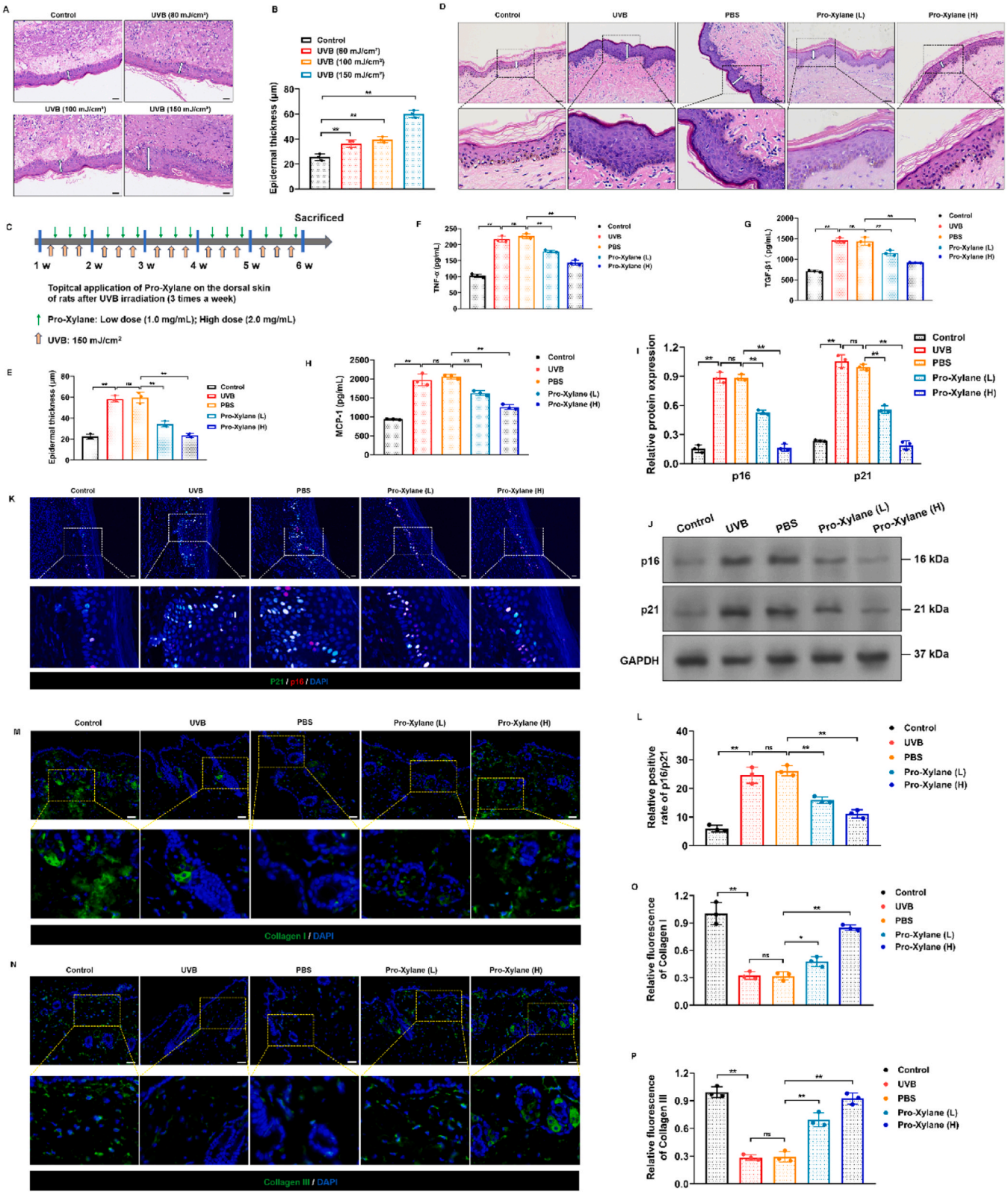

Fig. 6. Pro-Xylane ameliorates UVB-induced skin senescence and damage in vivo. (A-B) HE staining of rat skin sections and quantification of epidermal thickness (n = 3). Scale bar= 20 μm. (C) Schematic of the in vivo experimental protocol. (D) HE staining of rat skin sections with white arrow indicating the thickening of the epidermis (n = 3). Scale bar= 20 μm. (E) Quantification of epidermal thickness (n = 3). (F-H) Analysis of SASP factors (TNF-α, MCP-1, TGF-β1) using assay kits (n = 3). (I-J) Western blot assay of p21 and p16 (n = 3). (K-L) Double immunofluorescence staining and quantification for p21/p16 expression (n = 3). Scale bar= 20 μm. (M-P) Immunofluorescence staining and quantification for Collagen I, and Collagen III (n = 3). Scale bar= 20 μm. Data were presented as mean ± SD; **P < 0.01. ns=non-significant.

impaired tissue integrity (Tanveer et al., 2023). The present study systematically demonstrates that Pro-Xylane exerts robust protective effects against UVB-mediated skin injury both in vitro and in vivo, with its mechanisms centered on the inhibition of SGK1 and the regulation of p21 ubiquitination and subcellular localization.

First, our in vitro experiments with HaCaT cells revealed that UVB exposure significantly decreased cell viability, increased the rate of apoptosis, and elevated oxidative stress, all of which are hallmarks of UVB-induced skin damage. These results are consistent with previous studies (Gromkowska-Kępka et al., 2021; Salminen et al., 2022) showing that UVB radiation triggers cellular responses such as DNA damage, oxidative stress, and inflammation, leading to apoptosis and skin aging. The selection of 40 mJ/cm^2 as the optimal UVB dose, alongside evidence that Pro-Xylane (100–1000 μM) does not affect normal HaCaT viability, establishes a safe and relevant experimental framework. Notably, Pro-Xylane reversed UVB-induced reductions in cell viability, inhibited apoptosis, and mitigated oxidative stress—effects that align with its known role in enhancing skin barrier function (Bouloc et al., 2017) but extend its biological relevance to UVB-specific damage. Previous research reported that senescent cells can alter the tissue microenvironment by secreting SASP factors, which can also create a pro-inflammatory milieu (Kim et al., 2020). The TNFα (SASP factor) secretion from senescent cells promoted apoptosis in neighboring non-senescent cells as well as senescent cells themselves (Kim et al., 2020). Baar M, et al. found that FOXO4 potently and selectively reduces the viability of senescent cells by competing with FOXO4-p53 binding, thereby triggering release of active p53 to the cytosol and inducing cell-intrinsic apoptosis through caspase-3/7 (Baar et al., 2017). Both senescence and apoptosis contribute to photoaging and structural degradation. Pro-Xylane exhibits a general cytoprotective effect, preventing sublethally damaged cells from entering senescence, and suppressing the SASP factors secretion to rescue damaged cells from apoptosis. In vivo, this dual protection prevents acute epidermal disruption while preserving long-term tissue homeostasis. We selected TNF-α, MCP-1, and TGF-β1 as representative SASP factors because they are key mediators of UVB-induced skin inflammation and senescence: TNF-α and MCP-1 promote inflammatory cell recruitment and amplify the senescence response (Picos et al., 2025), while TGF-β1 is involved in collagen degradation and skin fibrosis (Shi et al., 2013). However, this selection is not based on an unbiased approach (e.g., RNA-seq), and thus may miss other key SASP factors (e.g., IL-6, IL-8, CXCL1) that are also involved in UVB-induced senescence. Future studies will use transcriptome sequencing to conduct unbiased screening of SASP factors regulated by Pro-Xylane, which will help to comprehensively understand the role of Pro-Xylane in regulating the senescent microenvironment and provide more targeted evidence for its protective mechanism.

A key novelty of this study lies in the identification of SGK1 as a critical mediator of Pro-Xylane's actions. GEO dataset analysis pinpointed SGK1 as a UVB- differential gene, and functional validation confirmed that Pro-Xylane suppresses SGK1 expression at both transcriptional and translational levels. SGK1, a stress-responsive kinase, is implicated in regulating cellular redox balance and inflammation (Lu et al., 2022; Wang et al., 2019), and our experiments demonstrated that SGK1 is indispensable for Pro-Xylane to exert anti-senescence, anti--apoptotic, and pro-collagen effects. This finding bridge Pro-Xylane's biological activity to a specific molecular target, expanding our understanding of its mechanism beyond glycosaminoglycan synthesis. However, it is important to emphasize that the specific mechanism by which Pro-Xylane suppresses SGK1 expression/activity remains unknown. Pro-Xylane, functioning as an inducer of glycosaminoglycan synthesis, may exert indirect regulatory effects on SGK1 through ECM-integrin signaling pathways. Prior research has demonstrated that SGK1 activation can occur via hepatocyte growth factor (HGF) and phosphoinositide 3-kinase (PI3K)-dependent pathways, as well as through integrin-mediated, PI3K-independent mechanisms (Shelly and Herrera, 2002). The activation of SGK1 can be facilitated by signaling pathways that govern cell survival and mediate cell-cell and cell-matrix interactions (Shelly and Herrera, 2002). However, these hypotheses remain to be verified in future studies, and clarifying the regulatory mechanism of Pro-Xylane on SGK1 will further enhance the depth of our findings. Further mechanistic exploration revealed that Pro-Xylane modulates p21, a master regulator of senescence, through dual pathways: subcellular localization and ubiquitination. Nuclear p21 is a key mediator of cell cycle arrest and cellular senescence (Yan et al., 2024b; Englund et al., 2023), while cytoplasmic p21 is inactive and can be ubiquitinated and degraded by the proteasome (Hwang et al., 2009). The nuclear accumulation of p21 leads to sustained cell cycle arrest and senescence (Abella et al., 2010). UVB-induced nuclear accumulation of p21 was reversed by Pro-Xylane, which promoted cytoplasmic retention of p21. Concurrently, Pro-Xylane enhanced p21 ubiquitination, with the K141 residue identified as a critical site for this modification. Ubiquitination typically marks proteins for degradation or functional sequestration (Horák, 2003; Li et al., 2022), suggesting that Pro-Xylane accelerates p21 turnover or impairs its nuclear translocation. Besides, it suggests that SGK1 may regulate p21 stability by influencing ubiquitination modifications targeting K141. Since Pro-Xylane is a xylose derivative, it does not act directly as a ubiquitin ligase. Our data suggest it acts via the suppression of SGK1 expression. We hypothesize that SGK1, when active (e.g., under UVB stress), may interact with E3 ubiquitin ligases (such as MDM2), preventing p21 ubiquitination. By downregulating SGK1, Pro-Xylane lifts this inhibition, allowing endogenous ligases to ubiquitinate p21 at the K141 residue. Future studies will focus on identifying the specific E3 ubiquitin ligase involved in this process.

In vivo validation in a rat model strengthens the translational relevance of our findings. Pro-Xylane ameliorated UVB-induced epidermal thickening and SASP factor upregulation, while restoring collagen synthesis. Although HE staining did not show obvious morphological changes in the dermal compartment, immunofluorescence staining of Collagen I/III (main components of the dermis) showed significant changes. These results align with the in vitro data, confirming that Pro-Xylane's protective effects extend to intact skin, supporting its potential as a topical agent for UVB-related skin disorders.

While our results are promising, it is important to acknowledge some limitations of the study. First, the in vitro experiments were conducted using HaCaT cells, which are a human keratinocyte cell line. Although these cells provide a relevant model for studying UVB-induced skin damage, they may not fully replicate the complex interactions occurring in the skin's multilayered structure. Future studies using ex vivo skin models and primary human cells could provide more physiologically relevant data. In addition, UVB radiation, with a shorter wavelength and higher energy, penetrates the epidermis to induce direct DNA mutagenesis, particularly the formation of cyclobutane pyrimidine dimers (CPDs) and 6–4 photoproducts (6–4PPs) (Pfeifer, 2020; Mallet et al., 2016). In our future study, we will further investigate the formation of pyrimidine dimers during the process of Pro-Xylane on UVB-induced skin aging and damage, which will reveal the regulatory effect of Pro-Xylane on DNA photodamage repair.

In conclusion, our study demonstrates that Pro-Xylane exerts significant protective effects against UVB-induced skin aging and damage. By modulating the SGK1 signaling pathway, reducing oxidative stress, preventing apoptosis, and promoting collagen synthesis, Pro-Xylane offers a promising strategy for protecting the skin from the harmful effects of UVB radiation. These findings provide a strong foundation for further research into the therapeutic potential of Pro-Xylane in the prevention and treatment of photoaging, offering a novel approach for enhancing skin health and longevity.

Ethics approval

This study was approved by the Ethics Committee of West China Hospital, Sichuan University (Approval No.: 250721003).

Funding

This work was financially supported by Sichuan Science and Technology Program (2025YFHZ0061).

CRediT authorship contribution statement

Ting Yan: Writing – original draft, Formal analysis. **Xiaofang Zhang:** Writing – original draft, Formal analysis. **Nan Huang:** Formal analysis, Data curation. **Tingting Wang:** Writing – review & editing, Funding acquisition, Data curation, Conceptualization.

Declaration of Competing Interest

The authors confirm no competing interests in this study.

Acknowledgments

We appreciate the assistance of our laboratory colleagues in this research.

Appendix A. Supporting information

Supplementary data associated with this article can be found in the online version at doi:10.1016/j.mad.2026.112194.

Data availability

Data will be made available on request.

References

Abbas, T., Dutta, A., 2009. p21 in cancer: intricate networks and multiple activities. Nat. Rev. Cancer 9 (6), 400–414. https://doi.org/10.1038/nrc2657.

Abdallah, F., Mijouin, L., Pichon, C., 2017. Skin immune landscape: inside and outside the organism. Mediat. Inflamm. 2017, 5095293. https://doi.org/10.1155/2017/5095293.

Abella, N., Brun, S., Calvo, M., Tapia, O., Weber, J.D., Berciano, M.T., Lafarga, M., Bachs, O., Agell, N., 2010. Nucleolar disruption ensures nuclear accumulation of p21 upon DNA damage. Traffic 11 (6), 743–755. https://doi.org/10.1111/j.1600-0854.2010.01063.x.

Baar, M.P., Brandt, R.M.C., Putavet, D.A., Klein, J.D.D., Derks, K.W.J., Bourgeois, B.R.M., Stryeck, S., Rijksen, Y., van Willigenburg, H., Feijtel, D.A., van der Pluijm, I., Essers, J., van Cappellen, W.A., van IJcken, W.F., Houtsmuller, A.B., Pothof, J., de Bruin, R.W.F., Madl, T., Hoeijmakers, J.H.J., Campisi, J., de Keizer, P.L.J., 2017. Targeted apoptosis of senescent cells restores tissue homeostasis in response to chemotoxicity and aging. Cell 169 (1), 132–147.e16. https://doi.org/10.1016/j.cell.2017.02.031.

Bar, O., Valiukevičienė, S., 2025. Skin aging and type I collagen: a systematic review of interventions with potential collagen-related effects. Cosmetics 12 (4), 129. https://doi.org/10.3390/cosmetics12040129.

Beak, S.M., Lee, Y.S., Kim, J.A., 2004. NADPH oxidase and cyclooxygenase mediate the ultraviolet B-induced generation of reactive oxygen species and activation of nuclear factor-kappaB in HaCaT human keratinocytes. Biochimie 86 (7), 425–429. https://doi.org/10.1016/j.biochi.2004.06.010.

Bouloc, A., Roo, E., Moga, A., Chadoutaud, B., Zouboulis, C.C., 2017. A compensating skin care complex containing pro-xylane in menopausal women: results from a multicentre, evaluator-blinded, randomized study. Acta Derm. Venereol. 97 (4), 541–542. https://doi.org/10.2340/00015555-2572.

Domaszewska-Szostek, A., Puzianowska-Kuźnicka, M., Kuryłowicz, A., 2021. Flavonoids in skin senescence prevention and treatment. Int. J. Mol. Sci. 22 (13), 6814. https://doi.org/10.3390/ijms22136814.

Dorf, N., Maciejczyk, M., 2024. Skin senescence—from basic research to clinical practice. Front. Med. 11, 1484345. https://doi.org/10.3389/fmed.2024.1484345.

Dou, Z., Hu, P.-R., Song, L.-L., Wang, Y.-C., Tang, H.-N., Weng, Z.-Q., Wang, Y.-J., Cai, Y.-Q., 2025. Extensive gene mining and facile engineering of a novel carbonyl reductase for asymmetric synthesis of anti-aging (S)-Pro-Xylane from d-xylose. Int. J. Biol. Macromol. 305, 140976. https://doi.org/10.1016/j.ijbiomac.2025.140976.

E-Fatima, J., Khan, F.I., Lai, D., 2025. Exploring serum and glucocorticoid-regulated kinase 1: a promising target for COVID-19 and atrial fibrillation treatment. Heart Rhythm O2 6 (5), 720–732. https://doi.org/10.1016/j.hroo.2025.02.015.

El Ghalbzouri, A., Commandeur, S., Rietveld, M.H., Mulder, A.A., Willemze, R., 2009. Replacement of animal-derived collagen matrix by human fibroblast-derived dermal matrix for human skin equivalent products. Biomaterials 30 (1), 71–78. https://doi.org/10.1016/j.biomaterials.2008.09.002.

Englund, D.A., Jolliffe, A., Aversa, Z., Zhang, X., Sturmlechner, I., Sakamoto, A.E., Zeidler, J.D., Warner, G.M., McNinch, C., White, T.A., Chini, E.N., Baker, D.J., van Deursen, J.M., LeBrasseur, N.K., 2023. p21 induces a senescence program and skeletal muscle dysfunction. Mol. Metab. 67, 101652. https://doi.org/10.1016/j.molmet.2022.101652.

Gromkowska-Kępka, K.J., Puścion-Jakubik, A., Markiewicz-Żukowska, R., Socha, K., 2021. The impact of ultraviolet radiation on skin photoaging — review of in vitro studies. J. Cosmet. Dermatol. 20 (11), 3427–3431. https://doi.org/10.1111/jocd.14033.

Ho, C.Y., Dreesen, O., 2021. Faces of cellular senescence in skin aging. Mech. Ageing Dev. 198, 111525. https://doi.org/10.1016/j.mad.2021.111525.

Horák, J., 2003. The role of ubiquitin in down-regulation and intracellular sorting of membrane proteins: insights from yeast. Biochim. Biophys. Acta 1614 (2), 139–155. https://doi.org/10.1016/s0005-2736(03)00195-0.

Hwang, C.Y., Lee, C., Kwon, K.S., 2009. Extracellular signal-regulated kinase 2-dependent phosphorylation induces cytoplasmic localization and degradation of p21Cip1. Mol. Cell Biol. 29 (12), 3379–3389. https://doi.org/10.1128/MCB.01758-08.

Jiang, D., Fu, C., Xiao, J., Zhang, Z., Zou, J., Ye, Z., Zhang, X., 2019. SGK1 attenuates oxidative stress-induced renal tubular epithelial cell injury by regulating mitochondrial function. Oxid. Med. Cell Longev. 2019, 2013594. https://doi.org/10.1155/2019/2013594.

Jiao, Q., Zhi, L., You, B., Wang, G., Wu, N., Jia, Y., 2024. Skin homeostasis: mechanism and influencing factors. J. Cosmet. Dermatol. 23 (5), 1518–1526. https://doi.org/10.1111/jocd.16155.

Kim, D.E., Dollé, M.E.T., Vermeij, W.P., Gyenis, A., Vogel, K., Hoeijmakers, J.H.J., Wiley, C.D., Davalos, A.R., Hasty, P., Desprez, P.Y., Campisi, J., 2020. Deficiency in the DNA repair protein ERCC1 triggers a link between senescence and apoptosis in human fibroblasts and mouse skin. Aging Cell 19 (3), e13072. https://doi.org/10.1111/acel.13072.

Kim, S.R., Park, J.W., Lee, B.H., Lim, K.M., Chang, T.S., 2023. Peroxiredoxin V protects against UVB-induced damage of keratinocytes. Antioxidants 12 (7), 1435. https://doi.org/10.3390/antiox12071435.

Li, Y., Li, S., Wu, H., 2022. Ubiquitination-proteasome system (UPS) and autophagy two main protein degradation machineries in response to cell stress. Cells 11 (5), 851. https://doi.org/10.3390/cells11050851.

Liu, B., Li, N., He, Z., Zhang, X., Duan, G., 2021. Emerging role of serum glucocorticoid-regulated kinase 1 in pathological pain. Front. Mol. Neurosci. 14, 683527. https://doi.org/10.3389/fnmol.2021.683527.

Liu, J., Zhao, L., Xing, X., Zhang, Y., Ji, B., Zhou, F., 2025. The effects and mechanism of collagen peptide and elastin peptide on photoaging of skin cells induced by ultraviolet radiation. Food Biosci. 68, 106405. https://doi.org/10.1016/j.fbio.2025.106405.

Lu, R.-q, Zhang, Y.-y, Zhao, H.-q, Guo, R.-q, Jiang, Z.-x, Guo, R., 2022. SGK1, a critical regulator of immune modulation and fibrosis and a potential therapeutic target in chronic graft-versus-host disease. Front Immunol. 13, 822303. https://doi.org/10.3389/fimmu.2022.822303.

Mallet, J.D., Dorr, M.M., Drigeard Desgarnier, M.C., Bastien, N., Gendron, S.P., Rochette, P.J., 2016. Faster DNA repair of ultraviolet-induced cyclobutane pyrimidine dimers and lower sensitivity to apoptosis in human corneal epithelial cells than in epidermal keratinocytes. PLoS One 11 (9), e0162212. https://doi.org/10.1371/journal.pone.0162212.

Michalak, M., 2023. Plant extracts as skin care and therapeutic agents. Int. J. Mol. Sci. 24 (20), 15444. https://doi.org/10.3390/ijms242015444.

Mieremet, A., Rietveld, M., Absalah, S., van Smeden, J., Bouwstra, J.A., El Ghalbzouri, A., 2017. Improved epidermal barrier formation in human skin models by chitosan modulated dermal matrices. PLOS One 12 (3), e0174478. https://doi.org/10.1371/journal.pone.0174478.

Nagase, T., Akase, T., Sanada, H., Minematsu, T., Ibuki, A., Huang, L., Asada, M., Yoshimura, K., Nagase, M., Shimada, T., Aburada, M., Nakagami, G., Sugama, J., 2013. Aging-like skin changes in metabolic syndrome model mice are mediated by mineralocorticoid receptor signaling. Aging Cell 12 (1), 50–57. https://doi.org/10.1111/acel.12017.

Panich, U., Sittithumcharee, G., Rathviboon, N., Jirawatnotai, S., 2016. Ultraviolet radiation-induced skin aging: the role of DNA damage and oxidative stress in epidermal stem cell damage mediated skin aging. Stem Cells Int 2016, 7370642. https://doi.org/10.1155/2016/7370642.

Pfeifer, G.P., 2020. Mechanisms of UV-induced mutations and skin cancer. Genome Instab. Dis. 1 (3), 99–113. https://doi.org/10.1007/s42764-020-00009-8.

Picos, A., Seoane, N., Campos-Toimil, M., Viña, D., 2025. Vascular senescence and aging: mechanisms, clinical implications, and therapeutic prospects. Biogerontology 26 (3), 118. https://doi.org/10.1007/s10522-025-10256-5.

Salminen, A., Kaarniranta, K., Kauppinen, A., 2022. Photoaging: UV radiation-induced inflammation and immunosuppression accelerate the aging process in the skin. Inflamm. Res. 71, 817–831. https://doi.org/10.1007/s00011-022-01598-8.

Shelly, C., Herrera, R., 2002. Activation of SGK1 by HGF, Rac1 and integrin-mediated cell adhesion in MDCK cells: PI-3K-dependent and -independent pathways. J. Cell Sci. 115 (Pt 9), 1985–1993. https://doi.org/10.1242/jcs.115.9.1985.

Shi, J.H., Guan, H., Shi, S., Cai, W.X., Bai, X.Z., Hu, X.L., Fang, X.B., Liu, J.Q., Tao, K., Zhu, X.X., Tang, C.W., Hu, D.H., 2013. Protection against TGF-β1-induced fibrosis effects of IL-10 on dermal fibroblasts and its potential therapeutics for the reduction of skin scarring. Arch. Dermatol. Res 305 (4), 341–352. https://doi.org/10.1007/s00403-013-1314-0.

Stasiewicz, A., Conde, T., Gęgotek, A., Domingues, M.R., Domingues, P., Skrzydlewska, E., 2023. Prevention of UVB induced metabolic changes in epidermal cells by lipid extract from microalgae nannochloropsis oceanica. Int. J. Mol. Sci. 24 (14), 11302. https://doi.org/10.3390/ijms241411302.

Tang, X., Yang, T., Yu, D., Xiong, H., Zhang, S., 2024. Current insights and future perspectives of ultraviolet radiation (UV) exposure: friends and foes to the skin and beyond the skin. Environ. Int. 185, 108535. https://doi.org/10.1016/j.envint.2024.108535.

Tanveer, M.A., Rashid, H., Tasduq, S.A., 2023. Molecular basis of skin photoaging and therapeutic interventions by plant-derived natural product ingredients: a comprehensive review. Heliyon 9 (3), e13580. https://doi.org/10.1016/j.heliyon.2023.e13580.

Wang, M., Xue, Y., Shen, L., Qin, P., Sang, X., Tao, Z., Yi, J., Wang, J., Liu, P., Cheng, H., 2019. Inhibition of SGK1 confers vulnerability to redox dysregulation in cervical cancer. Redox Biol. 24, 101225. https://doi.org/10.1016/j.redox.2019.101225.

Yan, J., Chen, S., Yi, Z., Zhao, R., Zhu, J., Ding, S., Wu, J., 2024b. The role of p21 in cellular senescence and aging-related diseases. Mol. Cells 47 (11), 100113. https://doi.org/10.1016/j.mocell.2024.100113.

Yan, J., Chen, S., Yi, Z., Zhao, R., Zhu, J., Ding, S., Wu, J., 2024a. The role of p21 in cellular senescence and aging-related diseases. Mol. Cells 47 (11), 100113. https://doi.org/10.1016/j.mocell.2024.100113.

Yang, F., Chen, C., Chen, R., Yang, C., Liu, Z., Wen, L., Xiao, H., Geng, B., Xia, Y., 2025. Unraveling the potential of SGK1 in osteoporosis: from molecular mechanisms to therapeutic targets. Biomolecules 15 (5), 686. https://doi.org/10.3390/biom15050686.

Zang, S., Chen, J., Chevalier, C., Zhang, J., Li, S., Wang, H., Li, J., Chen, Y., Xu, H., Sheng, L., Zhang, Z., Qiu, J., 2024. Holistic investigation of the anti-wrinkle and repair efficacy of a facial cream enriched with C-xyloside. J. Cosmet. Dermatol. 23 (12), 4017–4028. https://doi.org/10.1111/jocd.16489.

Zhang, Z., Tan, R., Xiong, Z., Feng, Y., Chen, L., 2025. Dysregulation of autophagy during photoaging reduce oxidative stress and inflammatory damage caused by UV. Front. Pharmacol. 16, 1562845. https://doi.org/10.3389/fphar.2025.1562845.

Zhao, C., Wu, S., Wang, H., 2025. Medicinal plant extracts targeting UV-induced skin damage: molecular mechanisms and therapeutic potential. Int. J. Mol. Sci. 26 (5), 2278. https://doi.org/10.3390/ijms26052278.